Nanoscale Advances

ROYAL SOCIETY OF CHEMISTRY

PAPER

View Article Online
View Journal | View Issue

Cite this: *Nanoscale Adv.*, 2023, **5**, 4881

Dipole moment as the underlying mechanism for enhancing the immobilization of glucose oxidase by ferrocene-chitosan for superior specificity non-invasive glucose sensing†

Jo-Han Ting,[a] Po-Chuan Lin,[b] Shivam Gupta,[a] Ching-Hao Liu,[a] Tzuhsiung Yang,[b] Chi-Young Lee,[a] Yi-Ting Lai *[cde] and Nyan-Hwa Tai *[a]

Non-invasive methods for sensing glucose levels are highly desirable due to the comfortableness, simplicity, and lack of infection risk. However, the insufficient accuracy and ease of interference limit their practical medical applications. Here, we develop a non-invasive salivary glucose biosensor based on a ferrocene-chitosan (Fc-Chit) modified carbon nanotube (CNT) electrode through a simple drop-casting method. Compared with previous studies that relied mainly on trial and error for evaluation, this is the first time that dipole moment was proposed to optimize the electron-mediated Fc-Chit, demonstrating sturdy immobilization of glucose oxidase (GO_x) on the electrode and improving the electron transfer process. Thus, the superior sensing sensitivity of the biosensor can achieve 119.97 μA mM^{-1} cm^{-2} in phosphate buffered saline (PBS) solution over a wide sensing range of 20–800 μM. Additionally, the biosensor exhibited high stability (retaining 95.0% after three weeks) and high specificity toward glucose in the presence of various interferents, attributed to the specific sites enabling GO_x to be sturdily immobilized on the electrode. The results not only provide a facile solution for accurate and regular screening of blood glucose levels *via* saliva tests but also pave the way for designing enzymatic biosensors with specific enzyme immobilization through fundamental quantum calculations.

Received 18th May 2023
Accepted 5th August 2023

DOI: 10.1039/d3na00340j

rsc.li/nanoscale-advances

1 Introduction

The International Diabetes Federation (IDF) reports that the number of people with diabetes was 534 million in 2021 and this number is expected to increase to approximately 784 million in 2045.[1,2] Diabetes is currently the ninth leading cause of death, with around 1.5 million people dying directly from the disease in 2019.[3] Early diagnosis and management of diabetes can be achieved through regular testing of blood sugar, but current sensing methods rely on invasive acupuncture to collect blood, making blood glucose testing inconvenient and increasing the risk of wound infection.[4] In addition, frequent blood collection throughout the day not only causes fingertip wounds that are difficult to heal but also decreases people's willingness to undergo blood sugar tests due to the tremendous pain and stress.[5] It is reported that over 40% of diabetics do not follow self-monitoring of blood glucose (SMBG) guidelines,[6] which may lead to delayed diagnosis and even severe diabetes complications, such as heart disease, diabetic ketoacidosis, vision loss, and bacterial or fungal infections.[7–9] Therefore, the development of a non-invasive glucose sensing technique is highly crucial for routine SMBG and comprehensive diabetes diagnosis and care.

Recent pioneering efforts have been made to exploit non-invasive blood glucose analysis using optical methods such as Raman,[10] fluorescence,[11] and near/mid-infrared range spectroscopy,[12] or electrochemical methods such as voltammetric and amperometric detection,[13–15] to analyze glucose in biofluids that are correlated with blood glucose concentration. Among all non-invasive blood glucose monitoring approaches, saliva has been shown to reflect blood glucose concentration and provide a simple, inexpensive, and fast measurement method.[16]

Multiple electronic glucose biosensors have been proposed for the selective detection of glucose in various biological fluids using carbon nanotubes (CNTs) due to their high electrical conductivity, corrosion resistance, and superior mechanical

[a]*Department of Materials Science and Engineering, National Tsing Hua University, Hsinchu, 300, Taiwan, ROC. E-mail: nhtai@mx.nthu.edu.tw*

[b]*Department of Chemistry, National Tsing Hua University, Hsinchu, 300, Taiwan, ROC*

[c]*Department of Materials Engineering, Ming Chi University of Technology, New Taipei City, 24301, Taiwan, ROC. E-mail: laieating@mail.mcut.edu.tw*

[d]*Center for Plasma and Thin Film Technologies, Ming Chi University of Technology, New Taipei City, 24301, Taiwan, ROC*

[e]*Biochemical Technology R&D Center, Ming Chi University of Technology, New Taipei City, 24301, Taiwan, ROC*

† Electronic supplementary information (ESI) available: Electroactive surface area calculation, Density Functional Theory (DFT) calculations, human saliva test, and related characterizations. See DOI: https://doi.org/10.1039/d3na00340j

properties.[14,17] However, the hydrophobicity and poor dispersibility of CNTs result in deficiencies in accuracy and bonding sites to enzymes (typically glucose oxidase, GO_x), making CNT-based biosensors inappropriate for low glucose concentrations (particularly in saliva, which has a lower glucose concentration than blood).[18]

To realize a biosensor with high sensitivity and a wide-sensing range of glucose concentration, we demonstrate a salivary glucose biosensor based on ferrocene-chitosan (Fc-Chit) modified CNTs on a screen-printed electrode (GO_x/Fc-Chit/CNTs/SPE) through a simple drop-casting process. Although the mechanism of enzymatically electric communication by Fc-Chit for biosensors is challenging due to the flexibility and diversification of chitosan, detailed investigations of optimizing Fc-Chit are scarce. Herein, we performed quantum chemical calculations and proposed dipole moment as an underlying mechanism to confirm our experimental data. The superior sensing sensitivity of 119.97 μA mM^{-1} cm^{-2} with high specificity and stability and human saliva glucose measurement demonstrate not only the feasibility of the non-invasive glucose biosensor but also a design strategy for other enzymatic biosensors.

2 Experimental

2.1 Materials

Screen-printed electrodes (SPE) were purchased from Zensor R&D Co. Chitosan (a low molecular weight compound with 75% deacetylation), D(+)-glucose (alpha), ethanol (≥99.8%), lactic acid (LA), potassium chloride (KCl), acetic acid, artificial saliva (used in medical and dental research), GO_x (from *Aspergillus niger*, 235 U mg^{-1}), and uric acid (UA) were all purchased from Sigma-Aldrich. Potassium ferricyanide ($K_3Fe(CN)_6$), ascorbic acid (AA), and ferrocenecarboxaldehyde were purchased from Duksan Pure, Honeywell Fluka, and Thermo Fisher Scientific, respectively. All chemicals were of analytical grade and used as received.

2.2 Preparation of CNT dispersion

To synthesize acid-treated CNTs, 1 g of multi-walled CNT powder was added to a solution containing HNO_3 and H_2SO_4 (in a volume ratio of 1 : 3). The mixture was sonicated for 10 min and then heated to 80 °C while stirring at 400 rpm for 2 h. Afterwards, the mixture was cooled down to room temperature and neutralized with deionized (DI) water through vacuum filtration. The resulting product was then dried in an oven at 80 °C overnight to obtain the acid-treated CNTs.

2.3 Preparation of ferrocene-modified chitosan

In this study, 1 g of chitosan powder was added to 99% ethanol and stirred for 10 min to ensure uniform chitosan dispersion. Thereafter, 0.50, 0.75, 1.00, and 1.25 g of ferrocenecarboxaldehyde were separately added to the chitosan suspension and heated with stirring at 100 °C for 8 h. The resulting products were collected using suction filtration with DI water to remove excess ferrocenecarboxaldehyde, followed by drying at 80 °C for several hours to obtain the Fc-Chit.

2.4 Preparation of GO_x/Fc-Chit/CNTs/SPE

The fabrication procedure of the proposed modified electrode is illustrated in Fig. 1a. First, the SPE substrate underwent air plasma treatment for 1.5 min to make its surface hydrophilic. Next, 20 μL of acid-treated CNT dispersion (1 mg mL^{-1} in DI water) was drop-cast on the electrode at 40 °C to produce CNTs/SPE. The electrode was then modified by drop-casting 1.5 μL of Fc-Chit solution (1 mg mL^{-1} in 1 wt% acetic acid) onto the CNTs/SPE at 40 °C to produce Fc-Chit/CNTs/SPE. To immobilize the enzyme, 3.5 μL of GO_x solution (15 mg mL^{-1} in DI water) was coated on the Fc-Chit/CNTs/SPE and dried under vacuum for 3 h. Following this, the electrode's surface was rinsed with DI water and then blow-dried using a nitrogen spray gun to remove excess enzymes and obtain GO_x/Fc-Chit/CNTs/SPE.

2.5 Characterization

Field-emission scanning electron microscopy (FESEM, Hitachi SU-8010), X-ray photoelectron spectroscopy (XPS, ULVAC-PHI PHI 5000 Versaprobe II), field-emission TEM (ULTRA-HRTEM, JEOL JEM-ARM200FTH), atomic force microscopy (AFM, Bruker Dimension ICON), Fourier transform infrared spectrometry (FTIR, Thermo Nicolet is5 FTIR), contact angle meter (FTA-1000B), and X-ray diffraction (XRD, Bruker D2 PHASER) were used to characterize the synthesized Fc-Chit and fabricated electrodes. A potentiostat/galvanostat electrochemical instrument (Autolab PGSTAT30&FRA2) with a three-electrode system was used to conduct the electrochemical experiments, including cyclic voltammetry (CV) and electrochemical impedance spectroscopy (EIS). The modified SPE was used as the working electrode, while the counter and reference electrodes on the SPE substrate were carbon and Ag/AgCl, respectively. For CV measurements, 4 mL of 5.0 mM $K_3Fe(CN)_6$ in 0.10 M KCl and phosphate buffered saline (PBS) (the formula of the PBS solution is shown in Table S1†) were both used as the electrolyte. On the other hand, 100.0 mM $K_3Fe(CN)_6$ in 0.10 M KCl aqueous solution was used to perform electrochemical impedance spectroscopy (EIS) analysis. The amplitude of the applied potential was 0.01 V at open circuit potential with a frequency range of 0.1–100 000 Hz. For glucose sensing, different concentrations of glucose in 4 mL PBS solution were prepared to evaluate the sensing performance of the SPEs.

3 Results and discussion

Fig. 1b illustrates the proposed GO_x/Fc-Chit/CNTs/SPE, which offers highly sensitive, specific, and low-detection-limit salivary glucose measurement. In this design, chitosan, a biomass obtained from partially deacetylated natural chitin, is selected for enzyme immobilization because of its biocompatibility, non-toxicity, sustainability, and multiple active sites on the surface.[19,20] The numerous amine ($-NH_2$) and hydroxyl groups (–OH) on chitosan can effectively immobilize GO_x, which subsequently catalyzes the oxidation of glucose. Furthermore, an

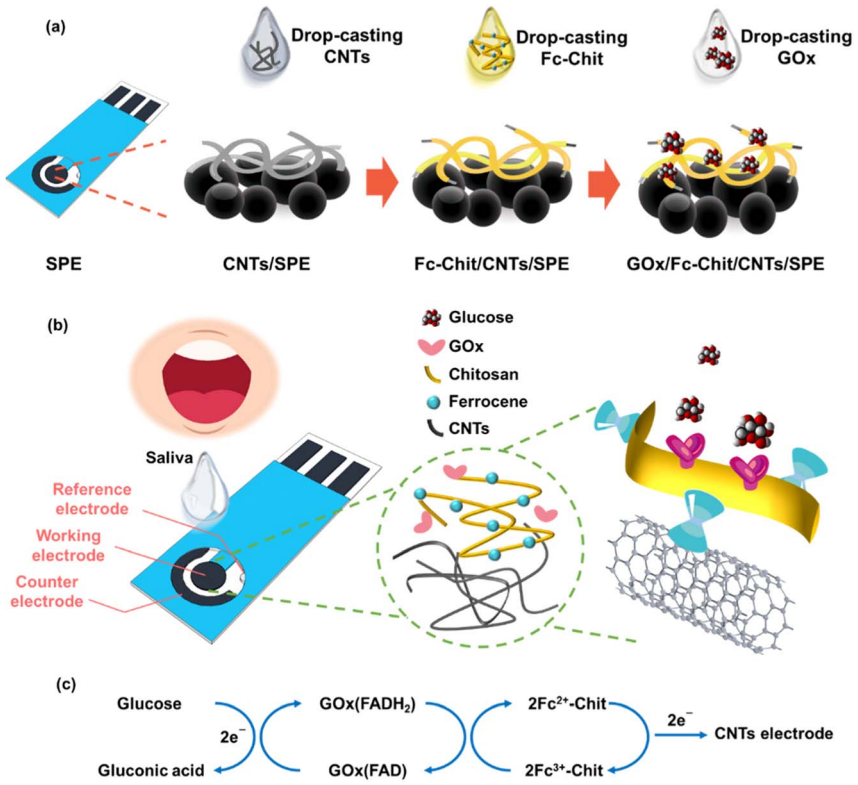

Fig. 1 Schematic illustration of the salivary glucose biosensor based on GO_x/Fc-Chit/CNTs/SPE. (a) The drop-casting fabrication sequence of the GO_x/Fc-Chit/CNTs/SPE. (b) The electrical current on the biosensor can be measured from the working to counter electrodes with Ag/AgCl as the reference electrode as it is exposed to salivary glucose. (c) For signal detection, oxidation of glucose triggered by GO_x can release electrons which can be immediately transferred to the CNT electrode by the redox Fc-Chit film.

electron-transfer mediator, ferrocene, is adopted to enhance electron transfer efficiency through the self-redox reaction.[21] It has been widely reported that the carboxyl and amine groups on GO_x can have electrostatic and hydrogen bonding interactions with chitosan.[22] Besides, the improved immobilization of the enzyme onto the electrode surface may result from the electrostatic interactions between enhanced positively charged Fc-Chit and negatively charged GO_x. The entanglement of the CNTs–chitosan structure can also facilitate the immobilization of GO_x by physical entrapment and adsorption, as reported by other studies.[23] Once exposed to fluid glucose, the anchored GO_x on the electrode surface can quickly catalyze the oxidation of glucose. During the enzymatic oxidation of glucose, the Fc-Chit serves as a redox mediator and facilitates the electron transfer to SPE, resulting in the augmentation of sensing performance (Fig. 1c).

FTIR spectroscopy was conducted to confirm the formation of Fc-Chit, as shown in Fig. S1.† The two characteristic peaks at 1642 and 1550 cm^{-1} can be attributed to the amide groups and the overlap of amide and amine groups on chitosan, respectively.[24] In Fc-Chit, the intensity of the peak at 1550 cm^{-1} for primary amine N–H bending decreases, while a new peak is observed at 823 cm^{-1}, which can be assigned to the cyclopentadiene of ferrocene.[25] The result indicates that *N*-alkylation of the glucosamine unit on chitosan with ferrocenecarboxaldehyde occurs, resulting in the formation of Fc-Chit. To investigate the mechanism of ferrocene attachment to chitosan, X-ray photoelectron spectroscopy (XPS) was further conducted to analyze the electronic structures of chitosan and Fc-Chit. The additional signal of Fe 2p in the Fc-Chit spectrum confirms that ferrocene is successfully grafted onto chitosan (Fig. S2†). In Fig. 2c, the N 1s photoelectron spectrum of chitosan shows a dominant peak at 399.4 eV, attributed to the NH_2 group.[26] The lower intensity peak (atomic ratio of 23.5%) at around 401.0 eV for N–C=O implies the presence of the acetylamine group, which is due to the incomplete deacetylation of chitin and is in agreement with the product report from Sigma-Aldrich (around 75% deacetylation).[27] It is worth noting that after introducing ferrocene, the ratio of NH_2 decreases from 73.5% to 25.1%. In contrast, a dominant peak at approximately 400.0 eV representing C–NH–C appears in Fc-Chit,[28] indicating that the formation process consumes the amino groups of chitosan and produces secondary amines between the ferrocene molecule and chitosan.[29] In addition, the increased intensity of protonated NH^{3+} groups at 401.5 eV indicates a proton transfer process from the covalent linking of C–NH–C to unreacted amino groups in Fc-Chit. Based on the above results, the aldehyde group of ferrocene can react with amine through the formation of Schiff bases, which are subsequently reduced to C–NH–C with the assistance of ethanol,[30,31] as illustrated in Fig. 2b.

To ensure that each layer in GO_x/Fc-Chit/CNTs/SPE was successively constructed using the facile drop-casting method,

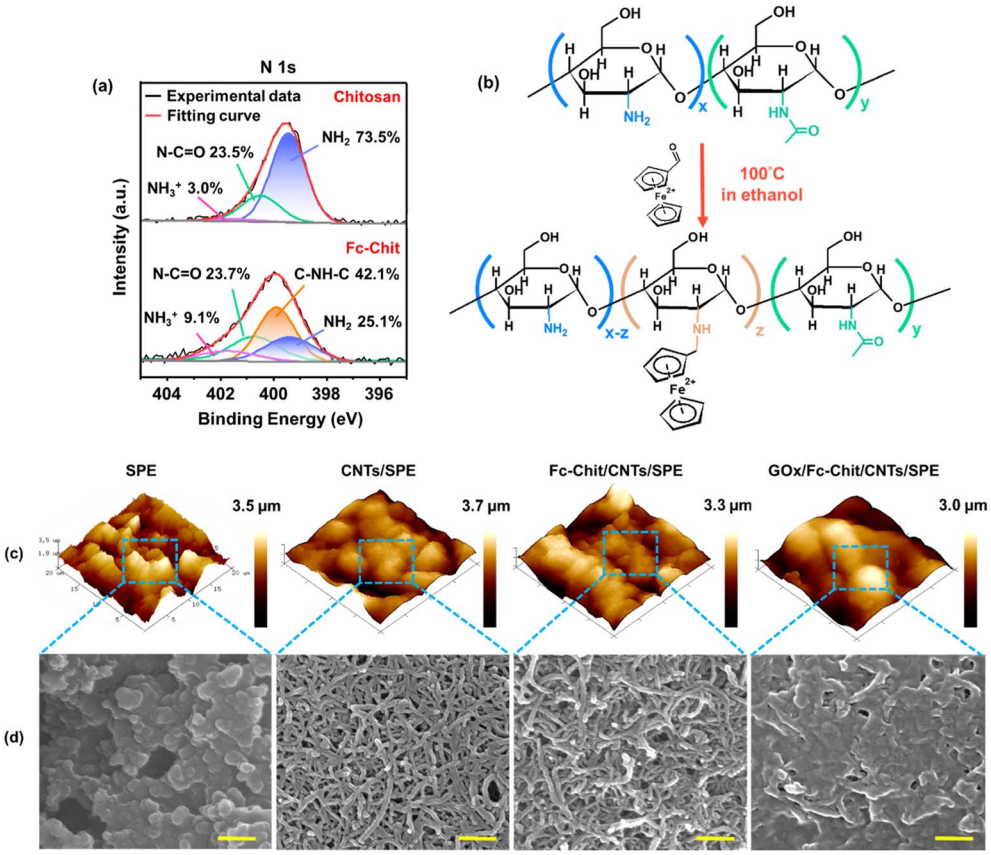

Fig. 2 Characterization of the formation of Fc-Chit on SPE. (a) XPS spectra of chitosan and Fc-Chit. (b) Schematic illustration of the synthesis of ferrocene-branched chitosan. (c) AFM images of each layer in GO_x/Fc-Chit/CNTs/SPE. The scanning area is 20 × 20 μm^2 for each sample. (d) SEM images of each layer in GO_x/Fc-Chit/CNTs/SPE. The yellow scale bar is 200 nm for each image.

AFM and SEM were used to characterize the variation of surface morphologies. Fig. 2c and d display the distinct particles on bare SPE, which are attributed to the carbonized polypropylene. Upon drop-casting the CNT dispersion, the CNTs are uniformly distributed, thereby reducing the roughness of the electrode surface (Table 1) (the optimization of CNT layers is provided in Fig. S3†). In Fig. 2d, multiple nano-sized pores can be observed, which are constructed by entangled CNT networks. The nanoporous structure of CNTs/SPE not only provides spaces for the subsequent Fc-Chit to penetrate but also facilitates ion transfer for glucose sensing.[32] As the Fc-Chit is introduced, the diameter of CNTs slightly increases while the pore size and number decrease (as depicted in Fig. S4†), indicating that CNTs are covered and wrapped by self-assembled Fc-Chit film. After the drop-casting of the enzyme, the surface of GO_x/Fc-Chit/CNTs/SPE is entirely covered by GO_x, and the morphology of CNTs can no longer be observed. As shown in Table 1, the decreased surface area can confirm that the gelatinous GO_x is successfully immobilized on the electrode.

To evaluate the ion diffusion behavior and sensing response of the electrodes, EIS was conducted in $K_3Fe(CN)_6$ solution to reveal the ion and charge transport dynamics (Fig. 3a). The Nyquist diagrams of each electrode exhibit an incomplete semicircle in the high-frequency region, followed by a 45°-incline caused by Warburg diffusion impedance (W_0).[33] In the equivalent circuit model, the equivalent series resistance (R_s) represents the combination of the solution resistance and the internal electrode resistance, which can be reflected by the intercept at the real part of impedance (X-axis).[34] The double-layer capacitance (CPE) is placed in parallel to a charge

Table 1 Comparison of morphology, R_s, and R_{ct} for electrodes with different modifications

Electrode	Average roughness (R_a, nm)	Root-mean-square roughness (R_q, nm)	Surface area (μm^2)	R_s (Ω)	R_{ct} (Ω)
SPE	420	525	554	133.3	338.9
CNTs/SPE	376	488	492	129.8	1.8
Fc-Chit/CNTs/SPE	362	474	490	135.2	2.2
GO_x/Fc-Chit/CNTs/SPE	389	472	426	141.6	4.4

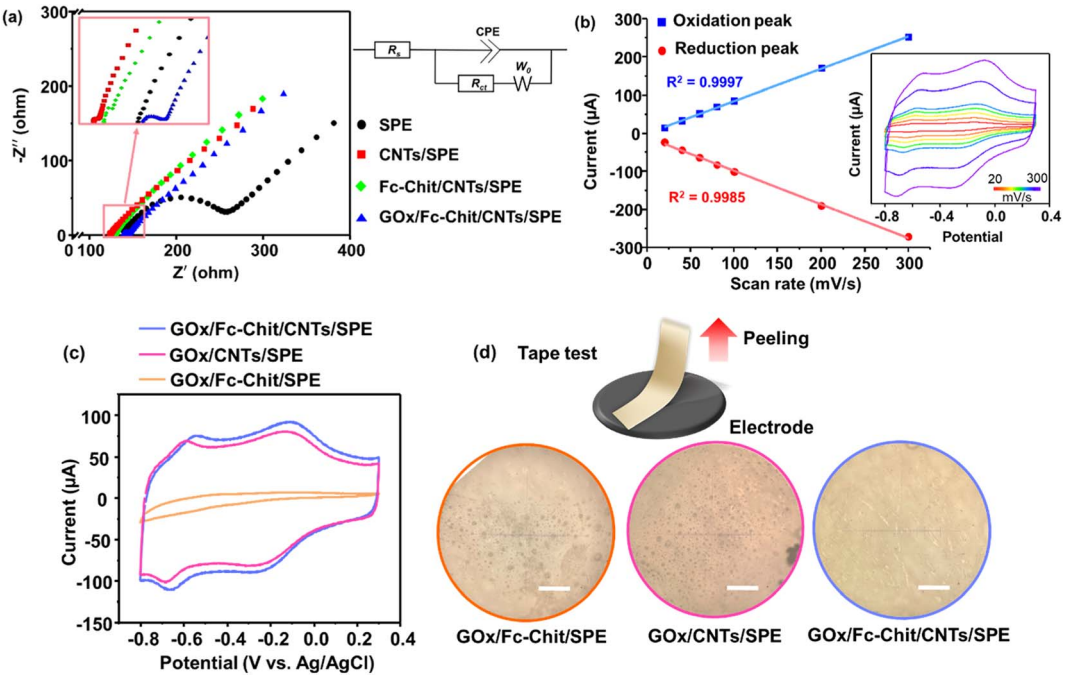

Fig. 3 Electrochemical characterization of each layer in GO_x/Fc-Chit/CNTs/SPE. (a) Nyquist diagrams of electrodes with different modifications with the equivalent circuit diagram, performed in 4 mL aqueous solution containing 100.0 mM $K_3Fe(CN)_6$ and 0.10 M KCl. The significant decrease in R_{ct} shows that the drop-casting of CNTs can effectively enhance the charge transfer process. (b) Plots of redox peak current *versus* scan rate derived from the inset of CV curves of GO_x/Fc-Chit/CNTs/SPE. The linear relationship between redox peak current and scan rate indicates a surface-controlled reaction of $GO_x(FADH_2)$ with dissolved O_2. The CV measurements were conducted using 4 mL PBS solution. (c) CV curves of CNTs and Fc-Chit modified SPE to evaluate the effects on the electrocatalytic redox of GO_x in PBS solution. (d) Optical microscopy images of the 3M tape after the tape test on modified SPEs. The white scale bar is 200 μm.

transfer resistance (R_{ct}). R_{ct} represents the interfacial resistance of the charge transfer between the electrolyte and electrode and can be described by the diameter of the semicircle. Here, both R_s and R_{ct} decrease after the drop-casting of the CNT dispersion, and in particular, R_{ct} decreases from 338.9 to 1.8 ohm (Table 1). This indicates that uniformly distributed conductive CNTs with numerous pores are beneficial for ion diffusion, hence effectively reducing the resistance of electron transport. In the subsequent modification using Fc-Chit and GO_x, both R_s and R_{ct} increase (as shown in Table 1). This can be attributed to the fact that the low-conductive Fc-Chit and GO_x films tend to clog the nanopores, hence hindering the access of ions to the electrode.

Fig. 3b shows the CV curves of GO_x/Fc-Chit/CNTs/SPE at various scan rates in the potential range of −0.30 to 0.60 V in PBS solution. The redox peak current increases linearly with the scan rate from 20 to 300 mV s^{-1}. The linear relationship between the redox peak current and scan rate indicates a surface-controlled process, which can be described by the following equation:[35]

$$I_p = \frac{n^2F^2vA\Gamma}{4RT} \quad (1)$$

where n is the number of electrons transferred during the reaction; F represents the Faraday constant (96 485 C mol^{-1}); Γ is the amount of reactant adsorbed; R is the ideal gas constant (8.314 J K^{-1} mol^{-1}); T is the absolute temperature (298 K); and A is the electroactive surface area (0.392 cm^2), which is determined from the Randles–Sevcik equation (Fig. S5†).[36] Considering n as 2, Γ can be derived to be 5.744×10^{-10} mol cm^{-2} in the reaction of $GO_x(FADH_2)$ with dissolved O_2 in PBS solution, as shown in the following equation:[37]

$$GO_x(FADH_2) + O_2 \rightleftharpoons GO_x(FAD) + H_2O_2 \quad (2)$$

where $FAD/FADH_2$ represents the redox catalysis of flavin adenine dinucleotide that can be observed in each subunit of GO_x.[38] The results show that integrating Fc-Chit and CNTs can provide a simple route for enhancing sensing performance.

To evaluate the impacts of each layer on the electrocatalytic redox of GO_x, GO_x was drop-cast on SPE with different modified layers for CV measurement in PBS solution. As shown in Fig. 3c, GO_x/Fc-Chit/SPE displayed minimal response in the potential window ranging from −0.80 to 0.30 V. Conversely, GO_x/CNTs/SPE exhibited apparent catalytic oxidation (−0.56 V) and reduction (−0.69 V) peaks. The shifting of the redox pair potentials is attributed to the overlap with the potential of the consumption of oxygen, which agrees with the results in previous works.[39,40] These results indicate that for the electrode with Fc-Chit alone, the redox center of GO_x is inadequate in electrical communication with the SPE surface due to the insufficient electrical conductivity, as confirmed by EIS (Table 1). In contrast, the presence of CNTs can effectively facilitate charge transfer in the redox reaction at the CNT-coated SPE. The redox peaks around −0.2 and 0 V, which only appeared in CV

curves in the presence of CNTs, may result from the redox reaction of hydroxyl ions on the carbon surface, as described in other literature reports.[41] Note that the highest redox peak currents and decreased peak-to-peak separation (ΔE_p) of 0.12 V can be observed for GO_x/Fc-Chit/CNTs/SPE, suggesting an efficient electrocatalytic process, however, which contradicts the higher R_{ct} observed by EIS (Table 1). These results aroused our interest in the effect of Fc-Chit on the electrocatalytic activity of GO_x. Although previous works have reported that ferrocene-branched chitosan can serve as a redox mediator and improve the attachment of GO_x to the electrode,[42,43] there is a lack of direct evidence to support this speculation. Therefore, an adherence test was performed by attaching 3M Scotch tape to the electrode surface and then peeling it off, as shown in Fig. 3d. Optical microscope images revealed that a significant amount of GO_x on GO_x/Fc-Chit/SPE and GO_x/CNTs/SPE was transferred to the 3M tape. However, with Fc-Chit as the intermediate layer, almost no GO_x was transferred from the electrode to the tape. The enhanced adhesion results from the strong electrostatic interactions between negatively charged acid-treated CNTs and positively charged Fc-Chit, allowing the latter to penetrate and cement the CNT layer (confirmed by Fig. 3d), thereby forming a robust film with numerous active sites to immobilize negative enzyme molecules for fluid glucose sensing.[24]

To optimize the sensing performance of GO_x/Fc-Chit/CNTs/SPE, we evaluated its glucose-responsive capability with different ratios of ferrocene-to-chitosan. Herein, predetermined amounts of ferrocenecarboxaldehyde were grafted to chitosan at branching ratios of 50, 75, 100, and 125% w/w and drop-cast onto the SPE to measure the sensitivity to fluid glucose at different concentrations in PBS. As shown in Fig. 4a, the cathodic current response decreases with an increase in glucose concentration, consistent with our previous works.[44] All GO_x/Fc-Chit/CNTs/SPEs with different ferrocene-to-chitosan ratios exhibit a reliable linear detection range of glucose concentration from 20 to 800 μM (Fig. S6†), covering the salivary glucose levels from 94 to 456 μM for healthy individuals and patients with diabetes,[45] respectively. Notably, GO_x/Fc-Chit/CNTs/SPE with a 75% ferrocene-to-chitosan ratio (0.75Fc-Chit) exhibits the highest sensitivity of 119.97 μA mM^{-1} cm^{-2} with a correlation coefficient of 0.9941 (Fig. 4b), elucidating the feasibility of the proposed biosensor for a non-invasive glucose sensing and management technique.

To gain a better understanding of our experimental data on the sensing performance with various ferrocene concentrations on an atomic scale, we performed quantum chemical calculations. Specifically, we calculated the dipole moments of the optimized geometries of Fc-Chit with one, two, or three condensations of FcCOOH on the 75% deacetylated chitosan backbone (which was obtained from Sigma-Aldrich) *via* the amine groups (abbreviated to Fc_1-Chit, Fc_2-Chit, and Fc_3-Chit, respectively). As shown in Fig. 4c, the 75% deacetylated chitosan backbone (referred to as the backbone) is composed of three chitosan and one chitin in the order of chitosan–chitin–chitosan–chitosan from C1 to C4. Additionally, we investigated three different regiomers for Fc_1-Chit and Fc_2-Chit, which we denoted as **1**, **2**, **3** and **4**, **5**, **6**, respectively. The results of these calculations are shown in Table 2.

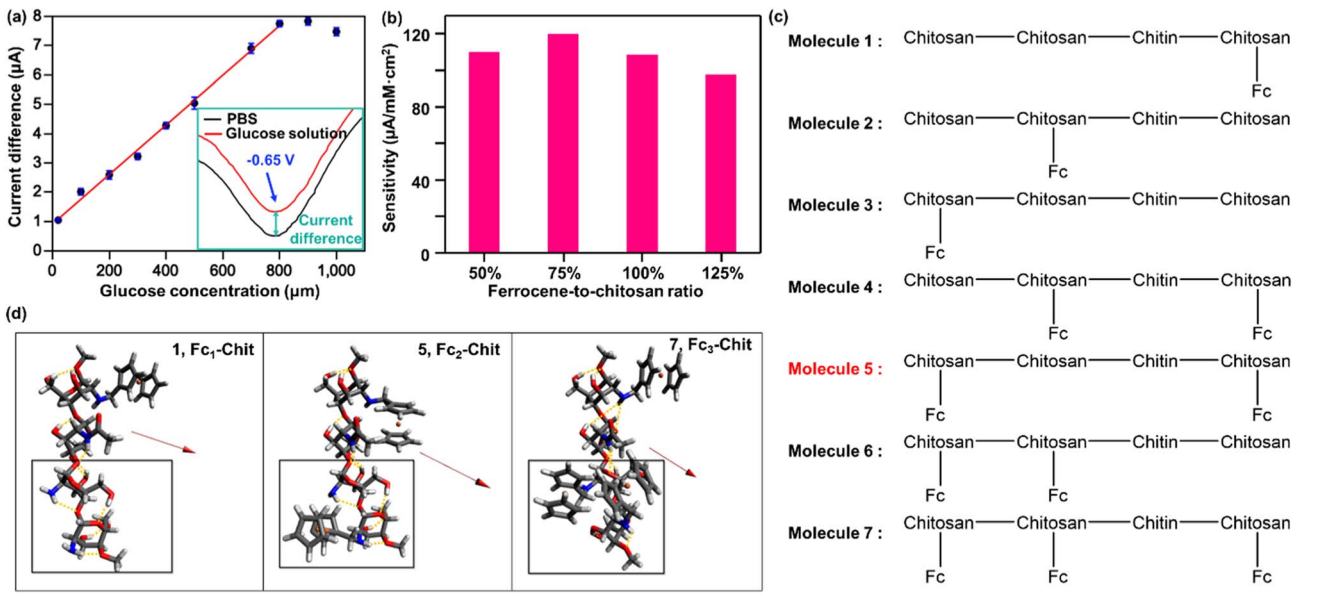

Fig. 4 Experimental results and theoretical explanation of the sensing performance enhancement by Fc-Chit modification. (a) Calibration curves of the current difference between the glucose concentration and enzyme reduction peak of GO_x/Fc-Chit/CNTs/SPE. (b) Glucose sensing sensitivity for biosensors modified with different ferrocene-to-chitosan branching ratios. (c) Representations of the optimized molecular structure of Fc-Chit molecules **1**–**7**, where molecule **5** possesses the highest total dipole moment of 3.05 (a.u.). (d) Illustrations of the optimized structures with the highest dipole moments among the regiomers of Fc_1-Chit (**1**, left), Fc_2-Chit (**5**, middle), and Fc_3-Chit (**7**, right). Hydrogen bonds within each molecule are labeled with yellow dashed lines. The red arrows indicate the dipole moment vectors starting at the center of mass and moving towards the direction with a more positive charge. The boxed regions are where structural reorganization occurs upon the condensation of FcCOOH with the NH_2-group of the third saccharide. Color code: H, white; C, grey; N, blue; O, red; Fe, orange.

Table 2 Total dipole moments (in units of a.u.) and their components in the *x*, *y*, and *z* directions for Fc_1-Chit (**1–3**), Fc_2-Chit (**4–6**), and Fc_3-Chit (**7**)

Molecule	1	2	3	4	5	6	7
Total dipole moment	2.75	2.24	2.30	2.53	3.05	1.88	2.15
Dipole moment (*x*)	0.24	0.42	0.19	0.19	0.41	0.58	0.70
Dipole moment (*y*)	1.94	0.63	−0.20	0.90	0.56	0.84	0.92
Dipole moment (*z*)	−1.94	−2.11	−2.29	−2.36	−2.97	−1.59	−1.82

Table 2 shows that among the Fc-Chit molecules investigated, Fc_2-Chit regiomer **5** exhibits the largest dipole moment, followed by Fc_1-Chit regiomer **1**. This finding is consistent with our experimental observation that 0.75Fc-Chit, which contains approximately 2.5 ferrocenes attached to the backbone by mass, exhibits the highest glucose sensing sensitivity of 119.97 μA mM^{-1} cm^{-2}. Interestingly, as the amount of ferrocene increases to 1.00Fc-Chit, which translates to 3.33 ferrocenes attached to the backbone (**7**), the glucose sensitivity decreases to 108.78 μA mM^{-1} cm^{-2}, in line with the lower calculated dipole moment of **7** compared to **5**. Initially, it was hypothesized that the sensing performance would improve with the number of ferrocenes attached to the backbone. However, the increased number of mobile electrons from ferrocene is counteracted by the reduced dipole moment, resulting in weaker binding to the acidic CNTs responsible for charge transfer to the electrode.

A closer look at the optimized structures of Fc-Chit regiomers **5** and **7** sheds light on the unexpected change in dipole moments upon increasing the number of ferrocenes attached to the backbone. Fig. 5c shows that the backbone in **5** retains the whole hydrogen bonding network as in **1**, Fc_1-Chit. However, upon the attachment of the third Fc at the third saccharide, as occurred in **7**, the bulky Fc substituent forces the fourth saccharide to rotate away from its optimal conformation, removing all the hydrogen bonding networks between the third and fourth saccharide units (boxed regions in Fig. 5c). This rotation hinders the alignment of the partial negative charges of the backbone, as seen in the dipole moment in the *z* direction in Table 2, reducing the total dipole moment of **7** (from −2.97 a.u. in **5** to −1.82 a.u. in **7**). This effect also transpires in **2**, **4**, and **6**, which are regiomers of Fc_1-Chit and Fc_2-Chit that have the third saccharide attached to a CH_2Fc unit (see the Density Functional

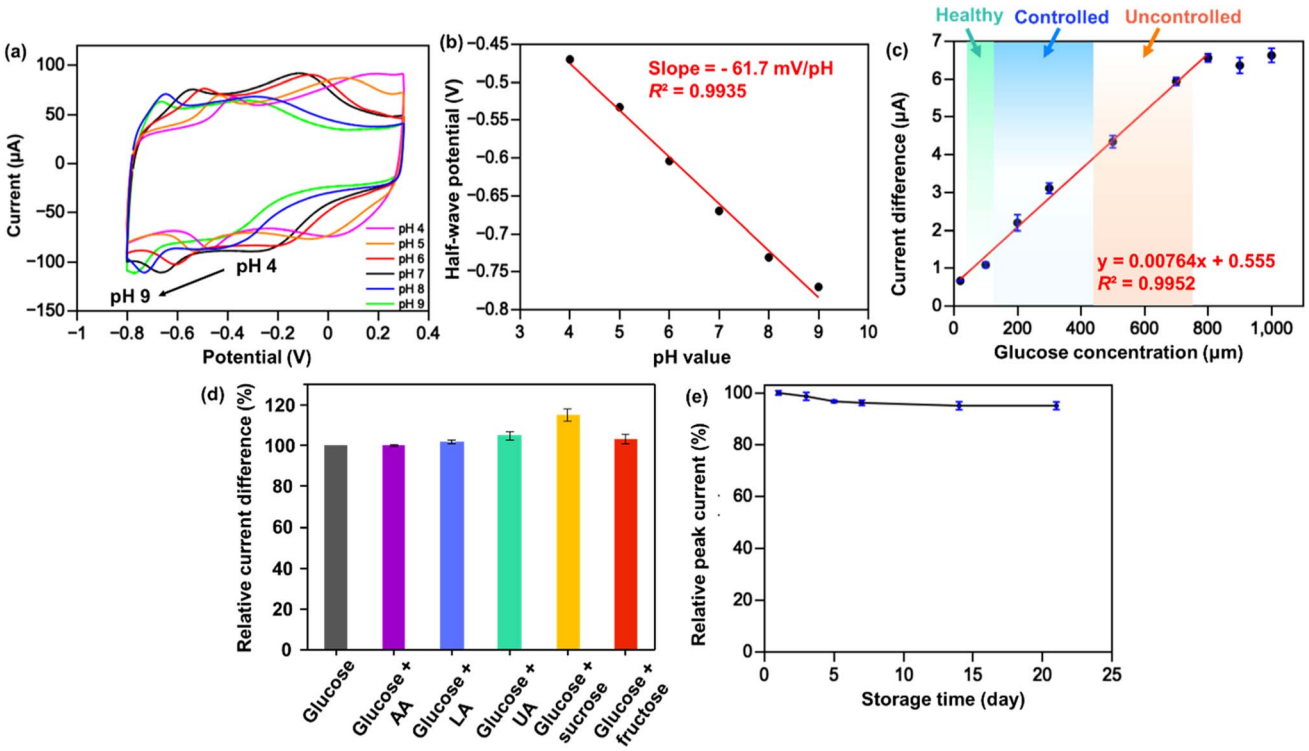

Fig. 5 The applicability evaluation of GO_x/Fc-Chit/CNTs/SPE. (a) CV curves of GO_x/Fc-Chit/CNTs/SPE in PBS solutions with various pH values at a scan rate of 100 mV s^{-1}. (b) Half-wave potential ($E_{1/2}$) profiles correspond to cathodic peak potential in (a) as a function of pH value. (c) Calibration curves of the current difference between the glucose concentration and enzyme reduction peak of the GO_x/Fc-Chit/CNTs/SPE in 75% artificial saliva. The salivary glucose levels of healthy individuals, well-controlled diabetics, and uncontrolled diabetics have been marked in green, blue, and orange colors, respectively. (d) Interference test of the GO_x/Fc-Chit/CNTs/SPES with 100 μM glucose and same additional concentration of interferents of AA, LA, UA, sucrose, and fructose. (e) Storage stability of the GO_x/Fc-Chit/CNTs/SPE for glucose sensing, which can retain 95.0% of the electrocatalytic activity after 3 weeks.

Theory (DFT) calculation section in the ESI†). A larger effect is observed when both the third and fourth saccharides are functionalized (**6** and **7**), due to the steric clash between the Fc on the third saccharide and both the fourth saccharide backbone and its Fc substituent. According to the experimental and simulated results, while ferrocene can facilitate electrochemical communication between the immobilized GO_x and the electrode surface, leading to more sensitive and stable biosensors, excessive ferrocene may obstruct the active sites of chitosan for the biocatalyst due to steric hindrance and prevent GO_x from anchoring on the electrode surface.[46] These findings not only provide a molecular-level understanding of the optimization of the proposed biosensor for glucose detection but also pave the way for designing other enzymatic biosensors through fundamental quantum calculations.

The pH-dependent behavior of the enzymatic redox current peaks is important to consider since enzymatic catalysis involves the transfer of protons and electrons,[47,48] which may impact the sensitivity and accuracy of glucose measurements. Therefore, it is crucial to ensure that the biosensor is stable and reliable under various pH conditions. In Fig. 5a, as the pH value increases, the half-wave potential ($E_{1/2}$) corresponding to FAD moves toward a more negative potential (the $E_{1/2}$ is −0.66 V at pH 7.0 and is −0.78 at pH 9.0). In contrast, the cathodic peak potentials for lower pH values move toward less negative ones (the $E_{1/2}$ is −0.47 V at pH 4.0). Furthermore, the enzymatic reduction peak potential is linearly proportional to the pH value in the pH range from 3 to 8 with the slope of -61.7 mV pH^{-1} (Fig. 5b), which is in accordance with the literature for a reversible redox process with two-proton/electron activity.[49] Using the Nernst equation can further validate the actual number of electrons involved in the reduction of FAD:[50]

$$\frac{dE}{d(pH)} = 2.303\frac{2RT}{nF} \quad (3)$$

here, E is the half-wave potential, and thus the number of electrons participating in the reaction can be obtained, $n = 1.89$. The result is close to the theoretical value for the two-electron/proton redox of FAD, as described in Fig. 1c and other literature.[39]

To evaluate the applicability of GO_x/Fc-Chit/CNTs/SPE in human salivary glucose sensing, actual glucose concentrations were measured in commercial artificial saliva. However, wide-ranging fluid viscosity is a vital issue in saliva samples, which can pose a challenge for practical glucose biosensor applications.[51] CV curves show a lower cathodic peak current with a negative-shifted potential for artificial saliva compared to that for PBS solution (Fig. S7a†), indicating an inefficient electron transfer process. To address this, the artificial saliva samples were diluted with PBS to 75% to demonstrate the sensing performance, as shown in Fig. 5c and S7b.† After dilution, the ΔE_p decreased to nearly 0.12 V, similar to that in the PBS solution, and exhibited a linear response in the range of 20–800 μM with high sensitivity of 108.21 μA mM^{-1} cm^{-2}. To assess the specificity of GO_x/Fc-Chit/CNTs/SPE for practical salivary glucose monitoring, various common interfering molecules, such as uric acid (UA), ascorbic acid (AA), lactic acid (LA), sucrose, and fructose were tested. The current difference of enzyme reduction peak was measured using 100 μM glucose with the same concentration of each interferent in PBS solution (Fig. 5d and S8†). Though a 15.2% increment of current difference can be observed for glucose solution with 100 μM sucrose, it was reported that the salivary sucrose clearance time could be completed within 20 min,[52,53] indicating little influence on salivary glucose measurement by the fabricated biosensor. Almost no distinction can be observed in the enzyme reduction peak current in the presence and absence of other interferents (<5%), indicating that the immobilized GO_x and glucose-specific electrocatalytic reaction allow for a highly specific and stable biosensor for fluid glucose.

The feasibility of using the GO_x/Fc-Chit/CNTs/SPE for human salivary glucose monitoring was demonstrated by measuring dynamic changes in salivary glucose concentration relating to diet. A healthy individual's saliva sample was tested, and the glucose concentration was calculated using standard glucose calibration (Fig. S9†). The results indicate that GO_x/Fc-Chit/CNTs/SPE can clearly reveal changes in salivary glucose concentration between postprandial and fasting conditions in the normal range.[54] The storage stability of GO_x/Fc-Chit/CNTs/SPE was investigated by measuring the average reduction peak current of 500 μM glucose after a predetermined number of days of storage in a vacuum at 4 °C. After being stored for three weeks, the GO_x/Fc-Chit/CNTs/SPE exhibited good stability, with the relative peak current remaining at 95.0% compared to the first day (Fig. 5e), and excellent operational stability with a standard deviation lower than 2.0%. The GO_x/Fc-Chit/CNTs/SPE shows better storage and operational stability than previous works using metal nanoparticles, polymerized ionic liquids, or metal oxide composites as biosensors.[55–57] The improved stability may result from the electrostatic interactions between the positively charged Fc-Chit and negatively charged GO_x and acid-treated CNT supporting layer, leading to a robust and rigid structure.

Moreover, the high biocompatibility of chitosan is reported to be an ideal enzyme fixative that can maintain protease activity during enzyme immobilization.[58] The porous structure of the entangled CNT layer also allows for the enzyme to form a 3D enzyme structure, thus enhancing the tolerance of the fabricated biosensor to environmental changes. Table 3 summarizes the sensing performance of the selected state-of-the-art chitosan or ferrocene-modified glucose biosensors. While some biosensors possess a wider linear sensing range than GO_x/Fc-Chit/CNTs/SPE, they require the use of metal/metal oxide components, leading to high costs and complicated fabrication processes. On the other hand, the proposed biosensor exhibits superior sensitivity that is one order of magnitude higher than most published results. Besides, this study showcases the integration of experimental and theoretical approaches to optimize biosensor design, in contrast to previous literature that relied mainly on data-driven evaluation through trial and error. These findings can lead to more efficient and effective biosensor development and advance practical applications in various fields.

Table 3 Comparison of the selected state-of-the-art glucose biosensors

Materials	Detection target	Linear range (mM)	Sensitivity ($\mu A\ mM^{-1}\ cm^{-2}$)	LOD[a] (μM)	Publishing year and reference
Fc-Chit/CNT@Cu/GCE	0.1 M NaOH solution	0.2–22	1.26	13.52	2020 (ref. 59)
Fe_3O_4-chitosan-β-cyclodextrin/MWCNTs	Human serum	0.04–1.04	23.59	19.30	2021 (ref. 60)
MPC-CHT-GO_x	Saliva, serum, and urine	0.25–3	56.12	4.1	2019 (ref. 61)
Chit/ZnO NPs/GCE	Grape juice	10–900	41.53	0.9	2020 (ref. 62)
AgNWs/CS/GOx	PBS solution	1–15	16.72	2.1	2016 (ref. 63)
CS-GO	Human dermal fibroblast cell	0.01–20	0.17	1.0	2019 (ref. 64)
CHIT(GO_x)/AuLr-TiND	Saliva, serum, and sweat	0.04–15.05	23.47	1.75	2021 (ref. 65)
GO_x/chitosan immobilized LIGE	PBS solution	0–8	43.15	0.43	2021 (ref. 66)
P(SNS-Fc-*co*-EDOT)/CNT	PBS solution	0.01–1.0	11.58	1.63	2020 (ref. 67)
GO_x/Fc-Chit/CNTs/SPE	**Saliva**	**0.02–0.8**	**119.97**	**20.0**	**This work**

[a] LOD: limit of detection.

4 Conclusion

In summary, we developed a simple drop-casting method to fabricate a non-invasive salivary glucose biosensor using Fc-Chit and CNTs. Compared with previous literature that relied mainly on data-driven evaluation through trial and error, this study showcases the integration of experimental and theoretical approaches for optimizing the ferrocene-to-chitosan branching ratio, achieving a significant sensing performance with high sensitivity of 119.97 $\mu A\ mM^{-1}\ cm^{-2}$ over a wide detection range of 20–800 μM. Evaluation of the applicability of the biosensor in practical salivary glucose measurement was confirmed by multiple experiments, including artificial saliva samples, interference, stability, and detection of dynamic changes in salivary glucose concentration related to diet. This work provides a simple and low-cost approach with direct and fundamental evidence for enhanced sensing performance, which can pave the way for designing biosensors with immobilization of other enzymes for various applications.

Author contributions

J. H. T., Y. T. L., and N. H. T. conceived the idea. J. H. T. prepared and characterized the samples. P. C. L. and T. Y. conducted the DFT calculations. C. H. L. helped conduct the tape tests and interference tests. J. H. T. and Y. T. L. mainly wrote the manuscript. All authors discussed the results and contributed to the writing of the paper.

Conflicts of interest

There are no conflicts to declare.

Acknowledgements

The authors are thankful for funding support from the Ministry of Science and Technology, Taiwan, under contract number MOST 109-2622-E-007-029. We also thank the National Science and Technology Council for funding support under contract number NSTC 111-2222-E-131-003-MY2 and NSTC 111-2113-M-007-031-MY3. Tzuhsiung Yang also acknowledges the support from the Yushan Young Scholar Program, under the Ministry of Education (MOE), Taiwan. We also thank Prof. Po-Yao Chang (Department of Physics, National Tsing Hua University) for his kind suggestion about quantum chemical calculations. We also thank National Tsing Hua University and Ming Chi University of Technology for the funding and facilities support.

References

1 R. Williams, S. Karuranga, B. Malanda, P. Saeedi, A. Basit, S. Besançon, C. Bommer, A. Esteghamati, K. Ogurtsova, P. Zhang and S. Colagiuri, *Diabetes Res. Clin. Pract.*, 2020, **162**, 108072.
2 H. Sun, P. Saeedi, S. Karuranga, M. Pinkepank, K. Ogurtsova, B. B. Duncan, C. Stein, A. Basit, J. C. N. Chan, J. C. Mbanya, M. E. Pavkov, A. Ramachandaran, S. H. Wild, S. James, W. H. Herman, P. Zhang, C. Bommer, S. Kuo, E. J. Boyko and D. J. Magliano, *Diabetes Res. Clin. Pract.*, 2022, **183**, 109119.
3 W. H. Organization, *Diabetes*, 2021, **https://www.who.int/health-topics/diabetes#tab=tab_1**.
4 J. M. Torpy, A. Burke and R. M. Glass, *J. Am. Med. Assoc.*, 2005, **294**, 2122.
5 L. Tang, S. J. Chang, C.-J. Chen and J.-T. Liu, *Sensors*, 2020, **20**, 6925.
6 D. Nicholas, K. A. Logan, Y. Sheng, J. Gao, S. Farrell, D. Dixon, B. Callan, A. P. McHale and J. F. Callan, *Int. J. Pharm.*, 2018, **547**, 244–249.
7 Y.-H. Chen, C.-C. Lu and H.-C. Chen, *J. Rheumatol.*, 2018, **45**, 286.
8 H. Teymourian, C. Moonla, F. Tehrani, E. Vargas, R. Aghavali, A. Barfidokht, T. Tangkuaram, P. P. Mercier, E. Dassau and J. Wang, *Anal. Chem.*, 2020, **92**, 2291–2300.
9 S. Colagiuri, *Diabetes Res. Clin. Pract.*, 2014, **104**, 1–52.
10 R. Pandey, S. K. Paidi, T. A. Valdez, C. Zhang, N. Spegazzini, R. R. Dasari and I. Barman, *Acc. Chem. Res.*, 2017, **50**, 264–272.

11 J. Sawayama, T. Okitsu, A. Nakamata, Y. Kawahara and S. Takeuchi, *iScience*, 2020, **23**, 101243.
12 M. Bariya, H. Y. Y. Nyein and A. Javey, *Nat. Electron.*, 2018, **1**, 160–171.
13 S. O. Pereira, N. F. Santos, A. F. Carvalho, A. J. S. Fernandes and F. M. Costa, *Nanomaterials*, 2021, **11**(8), 1893.
14 T. Chang, H. Li, N. Zhang, X. Jiang, X. Yu, Q. Yang, Z. Jin, H. Meng and L. Chang, *Microsyst. Nanoeng.*, 2022, **8**, 25.
15 H. Lee, Y. J. Hong, S. Baik, T. Hyeon and D.-H. Kim, *Advanced Healthcare Materials*, 2018, **7**, 1701150.
16 A. Kumar, T. Kumar, M. Bhargava, R. Raj, V. Vaibhav and J. Kishore, *J. Med. Life*, 2020, **13**, 235–240.
17 Y. Lin, F. Lu, Y. Tu and Z. Ren, *Nano Lett.*, 2004, **4**, 191–195.
18 M. Pundir, P. Prasher, K. Vasić, M. Leitgeb, A. Kumar, R. Prakash, Ž. Knez, J. K. Pandey and S. Kumar, *Colloid and Interface Science Communications*, 2021, **44**, 100506.
19 M. Mu, X. Liang, D. Chuan, S. Zhao, W. Yu, R. Fan, A. Tong, N. Zhao, B. Han and G. Guo, *Carbohydr. Polym.*, 2021, **264**, 118000.
20 A. A. Essawy and A. M. El-Nggar, in *Materials for Biomedical Engineering*, eds. V. Grumezescu and A. M. Grumezescu, Elsevier, 2019, pp. 279–308, DOI: DOI: **10.1016/B978-0-12-818415-8.00010-3**.
21 L. Fabbrizzi, *ChemTexts*, 2020, **6**, 22.
22 M. N. Morshed, N. Behary, J. Guan and V. A. Nierstrasz, *ACS Sustainable Chem. Eng.*, 2021, **9**, 8879–8894.
23 D. Ohayon, G. Nikiforidis, A. Savva, A. Giugni, S. Wustoni, T. Palanisamy, X. Chen, I. P. Maria, E. Di Fabrizio, P. M. F. J. Costa, I. McCulloch and S. Inal, *Nat. Mater.*, 2020, **19**, 456–463.
24 W. Yang, H. Zhou and C. Sun, *Macromol. Rapid Commun.*, 2007, **28**, 265–270.
25 X. Du, H. Jiang, X. Guo, L. Chen and T. Kang, *React. Funct. Polym.*, 2021, **169**, 105061.
26 K. L. Kostov, E. Belamie, B. Alonso and T. Mineva, *Bulg. Chem. Commun.*, 2018, **50**, 135–146.
27 M. Bürger and J. Chory, *Commun. Biol.*, 2018, **1**, 217.
28 A. Artemenko, A. Shchukarev, P. Štenclová, T. Wågberg, J. Segervald, X. Jia and A. Kromka, *IOP Conf. Ser.: Mater. Sci. Eng.*, 2021, **1050**, 012001.
29 Ö. Yılmaz, D. O. Demirkol, S. Gülcemal, A. Kılınç, S. Timur and B. Çetinkaya, *Colloids Surf., B*, 2012, **100**, 62–68.
30 E. Raczuk, B. Dmochowska, J. Samaszko-Fiertek and J. Madaj, *Molecules*, 2022, **27**, 787.
31 Y.-A. Li, Y.-J. Chen and N.-H. Tai, *Langmuir*, 2013, **29**, 8433–8439.
32 N. Ogihara, Y. Itou and S. Kawauchi, *J. Phys. Chem. Lett.*, 2019, **10**, 5013–5018.
33 Y.-T. Lai, W.-T. Liu, L.-C. Chung, P.-I. Liu, M.-C. Chang, R.-Y. Horng, L.-J. Chen, C.-Y. Lee and N.-H. Tai, *Adv. Mater. Technol.*, 2019, **4**, 1900213.
34 Z. Zhou, T. Liu, A. U. Khan and G. Liu, *Sci. Adv.*, 2019, **5**, eaau6852.
35 A. Rabti, W. Argoubi and N. Raouafi, *Microchim. Acta*, 2016, **183**, 1227–1233.
36 C. S. Rao Vusa, V. Manju, S. Berchmans and P. Arumugam, *RSC Adv.*, 2016, **6**, 33409–33418.
37 A. Chaubey and B. D. Malhotra, *Biosens. Bioelectron.*, 2002, **17**, 441–456.
38 Y. Wang, M. Sun, J. Qiao, J. Ouyang and N. Na, *Chem. Sci.*, 2018, **9**, 594–599.
39 S. O. Pereira, N. F. Santos, A. F. Carvalho, A. J. S. Fernandes and F. M. Costa, *Nanomaterials*, 2021, **11**, 1893.
40 M. Wooten, S. Karra, M. Zhang and W. Gorski, *Anal. Chem.*, 2014, **86**, 752–757.
41 S. Gu, C.-T. Hsieh, C.-P. Kao, C.-C. Fu, Y. Ashraf Gandomi, R.-S. Juang and K. D. Kihm, *Catalysts*, 2021, **11**, 101.
42 A. Fatoni, A. Numnuam, P. Kanatharana, W. Limbut, C. Thammakhet and P. Thavarungkul, *Sens. Actuators, B*, 2013, **185**, 725–734.
43 H. Zhou, W. Yang and C. Sun, *Talanta*, 2008, **77**, 366–371.
44 G.-K. Huang, S. Gupta, C.-Y. Lee and N.-H. Tai, *Diamond Relat. Mater.*, 2022, **129**, 109385.
45 Y. Du, W. Zhang and M. L. Wang, *J. Diabetes Sci. Technol.*, 2016, **10**, 1344–1352.
46 M. Yuan, I. Tanabe, J.-M. Bernard-Schaaf, Q.-Y. Shi, V. Schlegel, R. Schurhammer, P. A. Dowben, B. Doudin, L. Routaboul and P. Braunstein, *New J. Chem.*, 2016, **40**, 5782–5796.
47 S. B. Bankar, M. V. Bule, R. S. Singhal and L. Ananthanarayan, *Biotechnol. Adv.*, 2009, **27**, 489–501.
48 J. Yu, C. Qian, Y. Zhang, Z. Cui, Y. Zhu, Q. Shen, F. S. Ligler, J. B. Buse and Z. Gu, *Nano Lett.*, 2017, **17**, 733–739.
49 H. Wang, L. Luo, H. Yu and F. Peng, MWNTs Modified Glassy Carbon Biosensor for Glucose, *1st IEEE International Conference on Nano/Micro Engineered and Molecular Systems*, Zhuhai, China, 2006, pp. 246–249, DOI: **10.1109/NEMS.2006.334696**.
50 H. Wei and S. Omanovic, *Chem. Biodiversity*, 2008, **5**, 1622–1639.
51 B. L. Schulz, J. Cooper-White and C. K. Punyadeera, *Crit. Rev. Biotechnol.*, 2013, **33**, 246–259.
52 L. M. Sreebny, R. Chatterjee and I. Kleinberg, *Arch. Oral Biol.*, 1985, **30**, 269–274.
53 S. Karaoglanoglu, Z. Y. Duymus, N. Akgul, N. Ozdabak, N. Seven and F. Ozabacygil, *Asian Biomed.*, 2010, **4**, 475–478.
54 S. Gupta, M. T. Nayak, J. D. Sunitha, G. Dawar, N. Sinha and N. S. Rallan, *J. Oral Maxillofac. Pathol.*, 2017, **21**, 334–339.
55 X. Chu, D. Duan, G. Shen and R. Yu, *Talanta*, 2007, **71**, 2040–2047.
56 L. Luo, Q. Li, Y. Xu, Y. Ding, X. Wang, D. Deng and Y. Xu, *Sens. Actuators, B*, 2010, **145**, 293–298.
57 X. Chu, B. Wu, C. Xiao, X. Zhang and J. Chen, *Electrochim. Acta*, 2010, **55**, 2848–2852.
58 M. Hedström, F. Plieva, I. Y. Galaev and B. Mattiasson, *Anal. Bioanal. Chem.*, 2008, **390**, 907–912.
59 F. Wang, S. Hu, F. Shi, K. Huang and J. Li, *Polymers*, 2020, **12**, 2419.
60 L. Peng, Y. Luo, H. Xiong, S. Yao, M. Zhu and H. Song, *Electroanalysis*, 2021, **33**, 723–732.
61 P. Barathi, B. Thirumalraj, S.-M. Chen and S. Angaiah, *Microchem. J.*, 2019, **147**, 848–856.
62 P. Liu, L. Yin and X. Qi, *Int. J. Electrochem. Sci.*, 2020, **15**, 5821–5832.

63 S. Kumar-Krishnan, S. Chakaravarthy, A. Hernandez-Rangel, E. Prokhorov, G. Luna-Bárcenas, R. Esparza and M. Meyyappan, *RSC Adv.*, 2016, **6**, 20102–20108.
64 M. A. Kafi, A. Paul, A. Vilouras, E. S. Hosseini and R. S. Dahiya, *IEEE Sensor. J.*, 2019, **20**, 6794–6801.
65 W. Lipińska, K. Siuzdak, J. Karczewski, A. Dołęga and K. Grochowska, *Sens. Actuators, B*, 2021, **330**, 129409.
66 K. Settu, P.-T. Chiu and Y.-M. Huang, *Polymers*, 2021, **13**, 2795.
67 A. Altun, R.-M. Apetrei and P. Camurlu, *J. Electrochem. Soc.*, 2020, **167**, 107507.